Title

"Application of an anisotropic constitutive model for structured clay to seismic slope stability

Journal

Journal of Geotechnical and Geoenvironmental Engineering, 137(5)

Authors

Taiebat, Mahdi
Kaynia, Amir
Dafalias, Yannis

Publication Date

2011-05-01

Application of an Anisotropic Constitutive Model for Structured Clay to Seismic Slope Stability

Mahdi Taiebat, M.ASCE[1]; Amir M. Kaynia, M.ASCE[2]; and Yannis F. Dafalias, M.ASCE[3]

Abstract: The anisotropic nature of response and degradation of shear strength from the undisturbed condition to the remolded state are two fundamental and challenging aspects of response in some clay deposits. This paper presents a comprehensive, yet flexible and practical, version of the SANICLAY model and its application to a seismic slope-stability problem. The model is based on the well-known isotropic modified Cam-Clay model with two additional mechanisms to account for anisotropy and destructuration. The model has been efficiently implemented in a three-dimensional (3D) continuum, coupled, dynamic, finite-difference program. The program has been used to analyze the seismic response of clay slopes to gain better insight into the role of the previously mentioned parameters in real applications. Different aspects of the model, including anisotropy and destructuration, and their effects on the earthquake-induced strains and deformations in the slope have then been explored and presented. By providing a link between the model parameters and the soil's undrained shear strength, which is a well-known engineering parameter, a benchmark comparison has been made between the results of the present advanced model and those of an engineering approach. To this end, a modified Newmark sliding-block analysis has been used, in which the yield acceleration is gradually reduced as block sliding progresses during the earthquake. It is observed that although the two analyses display the same trends, the modified Newmark sliding-block method provides conservative results compared with those obtained from the developed simulation model.
DOI: 10.1061/(ASCE)GT.1943-5606.0000458.

CE Database subject headings: Constitutive models; Anisotropy; Clays; Numerical models; Seismic effects; Slope stability.

Author keywords: Constitutive model; Anisotropy; Structured clay; Destructuration; Numerical modeling; Seismic slope stability.

Introduction

Seismic failure of slopes and geotechnical structures has been a major cause of human and material losses and has been the subject of much research. In addition to the complexities related to the seismic excitation, the estimation of the dynamic and strength characteristics of soil has been a major challenge in numerical simulations. While studies on onshore applications have been ongoing for some time, the offshore industry has more recently shown increasing interest in research and development on problems related to ocean floor stability. Submarine slides are major threats to the integrity of offshore engineering structures because of large displacements and forces involved in such failures. In addition, seismically induced submarine landslides pose a high risk of tsunami generation, of major concern near highly populated coastal areas.

Traditional methods of seismic slope stability assessment are established on a quasi-static approach. In moderate to severe seismic regions, this approach usually indicates slope failure. In most such cases, however, the slope experiences some permanent displacements without failure. A more realistic approach is to allow for soil nonlinearity and set limits for acceptable displacements. For this purpose, one needs reliable computational tools. Such tools need to address a number of challenges, such as capabilities for three-dimensional (3D) analyses, dynamic loading, handling the boundary conditions in a realistic way, fully coupled solid-pore fluid interaction, and inclusion of structural elements. Last but not least is constitutive behavior of the soil matrix, which is the crucial part of a successful numerical simulation. One of the challenges in constitutive modeling of clay deposits is capturing the fundamental features, such as material anisotropy and destructuration effects.

The numerical approaches used for modeling nonlinear response in clays fall into two general groups of total stress-based and effective stress-based methods. The total stress-based models address the nonlinear stress-strain relationship by empirically fitting experimental data. These models usually satisfy the Masing rule (Masing 1926) and provide a continuous (e.g., Ramberg and Osgood 1943) or a piecewise linear (e.g., Iwan 1967; Mroz 1967) expression for the first loading curve. The basic disadvantage of these models is that the stress-strain response is decoupled from the pore-pressure generation, but this has made these models much simpler. Other models have been introduced to relate stress-strain parameters to the current level of excess pore-water pressure through empirical laws, on the basis of number of cycles (e.g., Finn et al. 1977) or the mobilized stress ratio (e.g., Puzrin et al. 1995). A recent comprehensive study on an empirical total stress based method that also takes into account the cyclic response of clays is presented and discussed in Andersen (2009). The effective stress-based models used for clays are mainly derived from the theory of elastoplasticity. The elastoplastic constitutive models

[1]Assistant Professor, Dept. of Civil Engineering, Univ. of British Columbia, Vancouver, BC, Canada V6T 1Z4 (corresponding author). E-mail: mtaiebat@civil.ubc.ca

[2]Discipline Leader, Earthquake Engineering, Norwegian Geotechnical Institute, P.O. Box 3930 Ullevaal Stadion, N-0806 Oslo, Norway. E-mail: amir.m.kaynia@ngi.no

[3]Professor, Dept. of Civil and Environmental Engineering, Univ. of California at Davis, Davis, CA 95616; and Dept. of Mechanics, Faculty of Applied Mathematical and Physical Sciences, National Technical Univ. of Athens, Zographou 15780, Greece. E-mail: jfdafalias@ucdavis.edu

Note. This manuscript was submitted on September 20, 2009; approved on October 6, 2010; published online on October 8, 2010. Discussion period open until October 1, 2011; separate discussions must be submitted for individual papers. This paper is part of the ***Journal of Geotechnical and Geoenvironmental Engineering***, Vol. 137, No. 5, May 1, 2011. ©ASCE, ISSN 1090-0241/2011/5-492–504/$25.00.

are incremental, and nonlinear solution schemes are needed. The sophistication of the constitutive laws together with the complex mechanism of solid-pore fluid interaction that results in generation (and dissipation) of pore-water pressure could impose significant demands on the computational effort, especially in generalized six-dimensional stress space.

In the present development, the nonlinear finite-difference code fast Lagrangian analysis of continua in three dimensions, or FLAC^{3D} (Itasca Consulting Group 2006), is selected as the main platform. FLAC^{3D} is a dynamic code that uses an explicit time-integration scheme, coupled solid-pore fluid interaction, and large strain formulation and is well suited for solving dynamic stability problems. Constitutive behavior of the soil matrix is characterized in this work by a simplified version of the simple anisotropic clay (SANICLAY) plasticity model (Dafalias 1986; Dafalias et al. 2006; Taiebat et al. 2010). This model accounts for a number of important aspects of material response, such as initial and induced anisotropy and destructuration, to capture the strain softening that exists in some marine clays. The SANICLAY model is efficiently integrated in FLAC^{3D}, and the model implementation is successfully verified for different stress paths. This model is used in numerical simulation of a seismic slope-stability problem. The importance of anisotropy and destructuration to the mechanism of accumulation of displacements in deep-sea slopes is highlighted.

The fundamental equations of the constitutive model are presented and explained in the next section. Some additional equations pertinent to the numerical implementation are derived and presented in detail in the "Numerical Implementation of the Model" section. The numerical implementation of the model in the framework of FLAC^{3D} is subsequently verified with a stand-alone constitutive driver prepared based on earlier works of Bardet and Choucair (1991). The section on "Numerical Simulations" is devoted to application of the resulting numerical framework for modeling a boundary value problem. The simulations presented in this section aim to illustrate the importance of the constitutive features on anisotropy and destructuration in this very simple and practical model for modeling the response of a sloping ground during a dynamic event. An attempt has been made to compare the presented analyses results with engineering techniques in the "Results and Discussion" section. To this end, a link has been made between the advanced parameters of this model and the widely used undrained shear strength parameter s_u. The performance of the model has been compared with the Newmark sliding-block method that is one of the common engineering techniques for seismic slope-stability analysis. The paper ends with concluding remarks on the significance of combining a simple and realistic constitutive model with an efficient and rigorous numerical framework for solving problems of interest in geotechnical earthquake engineering practice.

Mathematical Formulation of the Model

The constitutive model is constructed by extending the well-recognized modified cam-clay (MCC) model (Roscoe and Burland 1968), which has a simple and elegant formulation with clear physical interpretation. The MCC model is very popular and widely applied in relatively advanced analyses in geotechnical engineering, and it is one of the most widely used models other than very simple models like Mohr-Coulomb.

The present formulation takes advantage of the simple framework of MCC, and with perhaps the simplest possible approach, adds the very important features of anisotropy and destructuration. Each one of these important constitutive features can be deactivated, if so desired by the user, simply by selecting appropriate values for certain model constants. In this way, the developed model can be simplified back to the MCC model. The present formulation does not include some of the constitutive features that existed in earlier work of Taiebat et al. (2010), such as the nonassociated flow rule and frictional destructuration mechanism, trading slightly less accuracy in simulations for simplicity. The resulting model is simple and rational, yet significantly improves the MCC model in describing some essential features of response in natural clays. It is intended to become a tool for solution of boundary value problems encountered in geotechnical engineering.

In this section, σ and ε are generic symbols for the stress and strain tensors and their components. All stress components are considered effective, and, as usual in geomechanics, both stress and strain quantities are assumed positive in compression. The stress tensor σ can be analyzed in a hydrostatic $p = (tr\sigma)/3$ and a deviatoric component $\mathbf{s} = \sigma - p\mathbf{I}$, where tr denotes the trace and $\mathbf{I}$ is the identity tensor. Similarly, the strain tensor ε can be decomposed in a volumetric $\varepsilon_v = tr\varepsilon$ and a deviatoric component $\mathbf{e} = \varepsilon - \varepsilon_v(\mathbf{I}/3)$. Within the range of small deformations and rotations, the kinematical assumption of the additive decomposition of total strain rate into elastic and plastic parts is assumed, i.e., $\dot{\varepsilon} = \dot{\varepsilon}^e + \dot{\varepsilon}^p$. The superscripts e and p denote elastic and plastic parts, respectively, and a superposed dot denotes, henceforth, the material time derivative or the rate. The elastic strain rate is given by

$$\dot{\varepsilon}^e = \frac{\dot{\varepsilon}_v^e}{3}\mathbf{I} + \dot{\mathbf{e}}^e = \frac{\dot{p}}{3K}\mathbf{I} + \frac{\dot{\mathbf{s}}}{2G} \tag{1}$$

where the elastic bulk and shear moduli K and G are obtained from

$$K = \frac{p(1+e)}{\kappa}; \qquad G = \frac{3K(1-2\nu)}{2(1+\nu)} \tag{2}$$

where e = current void ratio; and κ and ν = slope of the rebound line in $e - \ln p$ and the Poisson's ratio, respectively.

For simplicity, an associated flow rule has been employed, giving a single expression $f = 0$ for the yield surface and the plastic potential. The plastic strain rate is given by

$$\dot{\varepsilon}^p = \langle L \rangle \frac{\partial f}{\partial \sigma} \tag{3}$$

where L = loading index. The expression provided for the plastic potential, which is the same for the yield surface here, owing to application of associative plasticity, is obtained from an assumption for the plastic work dissipation given in Dafalias (1986), in the form of

$$f = \frac{3}{2}(\mathbf{s} - p\alpha)\colon(\mathbf{s} - p\alpha) - \left(M^2 - \frac{3}{2}\alpha\colon\alpha\right)p(p_0 - p) = 0 \tag{4}$$

where the symbol : implies the inner product of two tensors (the trace of their product); the anisotropic variable α = dimensionless deviatoric tensor; and p_0 = scalar variable. The scalar M is the critical stress ratio and can be interpolated between its values M_c in compression and $M_e = mM_c$ in extension as a function of a Lode angle θ and by means of the proposition of Argyris et al. (1974) as

$$M = \Theta(\theta, m)M_c = \frac{2m}{(1+m) - (1-m)\cos 3\theta}M_c \tag{5a}$$

$$\cos 3\theta = \sqrt{6}tr\mathbf{n}^3; \qquad \mathbf{n} = \frac{\mathbf{r} - \alpha}{[(\mathbf{r} - \alpha)\colon(\mathbf{r} - \alpha)]^{1/2}} \tag{5b}$$

with $\mathbf{r} = \mathbf{s}/p$ the deviatoric stress ratio tensor.

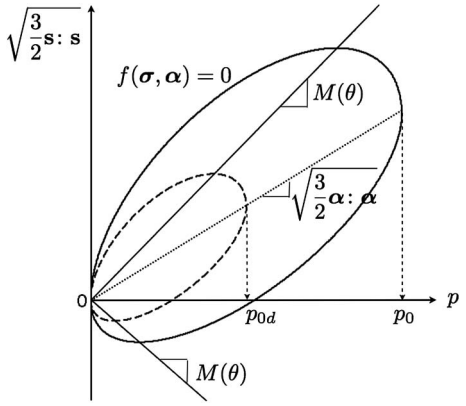

Fig. 1. Graphical representation of the SANICLAY model for structured clays in the stress space

A schematic illustration of $f=0$ is shown in Fig. 1, which is in essence the triaxial $p-q$ space. The isotropic hardening of the internal variable p_0 is based on the classical evolution law of critical state soil mechanics in conjunction with the specialization of Eq. (3) for the volumetric plastic strain rate and yields

$$\dot{p}_0 = \langle L\rangle\left(\frac{1+e}{\lambda-\kappa}\right)p_0 tr\left(\frac{\partial f}{\partial\sigma}\right) = \langle L\rangle\bar{p}_0 \tag{6}$$

The kinematic hardening rule for the internal variable α is based on the distance of back stress ratio α from its bounding *image* α^b, which in turn is defined by an *attractor* term $\mathbf{r}/x$ as (Dafalias et al. 2006; Taiebat et al. 2010)

$$\dot{\alpha} = \langle L\rangle\left(\frac{1+e}{\lambda-\kappa}\right)C\left(\frac{p}{p_0}\right)^2\left|tr\left(\frac{\partial f}{\partial\sigma}\right)\right|\left[\frac{3}{2}(\mathbf{r}-x\alpha):(\mathbf{r}-x\alpha)\right]^{1/2} \times(\alpha^b-\alpha) = \langle L\rangle\bar{\alpha} \tag{7a}$$

$$\alpha^b = \sqrt{\frac{2}{3}}M_e\mathbf{n}_x; \qquad \mathbf{n}_x = \frac{\mathbf{r}-x\alpha}{[(\mathbf{r}-x\alpha):(\mathbf{r}-x\alpha)]^{1/2}} \tag{7b}$$

where C and x = two model constants and the expression for $\bar{\alpha}$ is evident from the last two members of Eq. (7a). The constant C controls the evolution of anisotropy in the model, and the constant x in the attractor term provides a flexibility to the model for proper estimation of the value of K_0.

To include an isotropic destructuration mechanism in the model, the internal variable p_0 is set equal to $S_i p_{0d}$, where $S_i \geq 1$ is the isotropic structuration factor and p_{0d} is the destructured value of p_0 (or the value of p_0 at $S_i=1$). A slight difference of notation is adopted here from the work of Taiebat et al. (2010), whereas instead of p_0 and p_{0d}, the notations were p_0^* and p_0, respectively, were used. With this new definition of p_0, Eq. (6) should now be replaced by the following Eq. (8), where $p_0 = S_i p_{0d}$ yields

$$\dot{p}_0 = S_i\dot{p}_{0d} + \dot{S}_i p_{0d} = \langle L\rangle(S_i\bar{p}_{0d} + \bar{S}_i p_{0d}) = \langle L\rangle\bar{p}_0 \tag{8}$$

where the analytical expression of $\bar{p}_0$ is evident for the last two members of Eq. (8). Here $\bar{p}_{0d}$ and $\bar{S}_i$ are obtained from

$$\dot{p}_{0d} = \langle L\rangle\left(\frac{1+e}{\lambda-\kappa}\right)p_{0d} tr\left(\frac{\partial f}{\partial\sigma}\right) = \langle L\rangle\bar{p}_{0d} \tag{9a}$$

$$\dot{S}_i = -\langle L\rangle k_i\left(\frac{1+e}{\lambda-\kappa}\right)(S_i-1)\bar{\varepsilon}_d^p = \langle L\rangle\bar{S}_i \tag{9b}$$

with $\bar{p}_{0d}$ and $\bar{S}_i$ following from the last two members of Eqs. (9a) and (9b), respectively, and where k_i = material constant. The degradation of S_i has been taken into account by means of $\dot{\varepsilon}_d^p = \langle L\rangle\bar{\varepsilon}_d^p$, which is the rate of an auxiliary internal variable called the destructuration plastic strain rate and defined as

$$\dot{\varepsilon}_d^p = \langle L\rangle\bar{\varepsilon}_d^p = \sqrt{(1-A)\dot{\varepsilon}_v^{p2} + A\left(\frac{2}{3}\dot{\mathbf{e}}^p:\dot{\mathbf{e}}^p\right)} \tag{10}$$

The parameter A is a material constant distributing the effect of volumetric and deviatoric plastic strain rates to the value of $\dot{\varepsilon}_d^p$. The foregoing destructuration mechanism described by Eqs. (8)–(10) is a classical approach of isotropic destructuration introduced earlier by Nova (1992) and Gens and Nova (1993). In Taiebat et al. (2010), in addition to the present isotropic destructuration mechanism that is in effect an isotropic-softening constitutive feature, an additional frictional destructuration mechanism was introduced that addressed the possible collapse of the critical state stress ratio M in the foregoing destructuration plastic strain rate of Eq. (10). This mechanism is omitted in the present work for simplicity and because the isotropic destructuration is by far the more important of the two. In other words, many of the aspects of destructuration response in clays can be sufficiently addressed only by the isotropic destructuration mechanism for many practical purposes, and this approach has been adopted in the present work. Moreover, in Taiebat et al. (2010), the full destructuration model also had additional features, such as a plastic potential surface different than the yield surface with a different rotational variable, and simplified versions were studied in regard to simulations of data and the relative effect of the two aforementioned destructuration mechanisms was evaluated. It is on the basis of these studies and comparisons that the single-surface simplified version without the frictional destructuration is being considered in this paper without the need to repeat any data simulations, for which the reader is referred to Taiebat et al. (2010). To avoid any misunderstanding, it should be emphasized that the omission of the frictional destructuration implies only that the M remains intact, whereas the deviatoric (shear) strain rate is clearly influential in regard to the isotropic destructuration since it enters the definition of the destructuration plastic strain rate of Eq. (10), where A is different from zero with a typical default value of $A=0.5$.

Observe that by setting $C=0$ and starting with $\alpha=0$, the anisotropy feature of the model can be deactivated [see Eq. (7a)]. The destructuration mechanism can also be deactivated by setting $k_i=0$ or simply by starting with $S_i=1$ [see Eqs. (8) and (9)]. To fully reduce the model to the MCC model, in addition to the previous choices, one should also remove the Lode angle dependency by setting $m=1$ [see Eq. (5)].

Numerical Implementation of the Model

In this study, the SANICLAY model with destructuration, in its simple form presented in the previous section, has been numerically implemented in the 3D explicit finite-difference program FLAC^{3D} through its UDM option. The constitutive model is written in C++ and compiled as a dynamic link library (DLL) file that can be loaded whenever it is needed.

Accuracy of the numerical implementation of a constitutive model in a numerical framework is tied to the integration scheme employed. Various numerical techniques—explicit, refined explicit, and implicit—have already been proposed and extensively discussed in the literature (e.g., see Potts and Gens 1985; Sloan 1987; Borja and Lee 1990; Crisfield 1991; Borja 1991; Jeremić

and Sture 1997; Sloan et al. 2001). Implicit integration is the most accurate approach, and in most cases, a robust integration of a constitutive model dictates the use of an implicit algorithm. This, however, could be computationally complex and run-time extensive, in particular for more advanced constitutive models. The choice of the most efficient algorithm in combination with the overall computational burden may depend on the constitutive law and the numerical code in which it will be implemented. Because of the explicit nature of the global solution algorithm used in FLAC^{3D}, use of very small increments is the prerequisite for computational stability of the global solution. Given such a requirement in the main algorithm of this code, it has been decided to use a compatible stress update algorithm. To enhance the numerical accuracy, an explicit integration scheme with a drift-correction method and an optional substepping technique (Sloan 1987; Sloan et al. 2001) have been adopted for the model implementation in the current work.

Given a strain increment, the core of a constitutive driver for a general elastoplastic model is the following equation:

$$\dot{\sigma} = \mathbf{C}^{ep}\dot{\varepsilon} = \left[\mathbf{C}^e - h(L)\frac{(\mathbf{C}^e\colon \partial g/\partial\sigma) \otimes (\partial f/\partial\sigma\colon \mathbf{C}^e)}{K_p + \partial f/\partial\sigma\colon \mathbf{C}^e\colon \partial g/\partial\sigma}\right]\colon \dot{\varepsilon} \quad (11)$$

where the symbol $\otimes$ implies the tensor product of two tensors; the $h(L)$ = unit step function of L; g = plastic potential, and the expression of loading index L in terms of strain increment (rather than stress increment) is as follows:

$$L = \frac{\partial f/\partial\sigma\colon \mathbf{C}^e\colon \dot{\varepsilon}}{K_p + \partial f/\partial\sigma\colon \mathbf{C}^e\colon \partial g/\partial\sigma} \quad (12)$$

The present form of the SANICLAY model has an associated flow rule, i.e., $\partial f/\partial\sigma = \partial g/\partial\sigma$. On the basis of Eqs. (4) and (5) this derivative can be computed as follows:

$$\frac{\partial f}{\partial\sigma} = 3(\mathbf{s} - p\sigma) + \frac{1}{3}p\left(M^2 - \frac{3}{2}\mathbf{r}\colon \mathbf{r}\right)\mathbf{I} + \frac{\partial f}{\partial\theta}\frac{\partial\theta}{\partial\sigma} \quad (13a)$$

$$\frac{\partial f}{\partial\theta} = 6M^2p(p_0 - p)\left(\frac{1-m}{2m}\right)\Theta(\theta, m)\sin 3\theta \quad (13b)$$

$$\frac{\partial\theta}{\partial\sigma} = \frac{-3\left[\mathbf{n}^2 - (tr\mathbf{n}^3)\mathbf{n} - \frac{1}{3}\mathbf{I}(1 + tr(\mathbf{n}^2\alpha) - tr\mathbf{n}^3 tr(\mathbf{n}\alpha))\right]}{p[(3/2)(\mathbf{r}-\alpha)\colon (\mathbf{r}-\alpha)]^{1/2}\sin 3\theta} \quad (13c)$$

The plastic modulus K_p in Eqs. (11) and (12) acquires the following form from the consistency condition $\dot{f} = 0$ in conjunction with Eqs. (7*a*) and (8)

$$K_p = -\frac{\partial f}{\partial\alpha}\colon \bar{\alpha} - \frac{\partial f}{\partial p_0}\colon \bar{p}_0 \quad (14)$$

where

$$\frac{\partial f}{\partial p_0} = -p\left(M^2 - \frac{3}{2}\alpha\colon \alpha\right) \quad (15)$$

$$\frac{\partial f}{\partial\alpha} = -3p(\mathbf{s} - p\alpha) + 3p(p_0 - p)\alpha \quad (16)$$

The integration algorithm requires finding the point of transition from elastic to elastoplastic behavior, for which the equation $f(\sigma + x\dot{\sigma}^e) = 0$ should be solved for x. For the present yield surface function, this equation has been solved using an iterative scheme described in Crisfield (1991). After computing the intersection point $\sigma + x\dot{\sigma}^e$, the remaining portion of the strain increment, which is $(1-x)\dot{\sigma}^e$, was treated in an elastoplastic manner. The error associated with this assumption in the presence of nonlinear elasticity is tolerable with the small increments of loading used in the explicit integration of FLAC^{3D}.

To verify details of the implementation of the SANICLAY model in FLAC^{3D} and its communication with the rest of the code, this model is also implemented in a stand-alone constitutive driver in *MATLAB*. This constitutive driver is prepared based on a linearized integration algorithm for incremental constitutive equations, a technique proposed by Bardet and Choucair (1991). The implementation is conducted using a refined explicit integration of the constitutive model. The numerical performance of the model has been tested comprehensively under different loading conditions in both codes to make sure the results are consistent and the model is correctly communicating with the rest of the FLAC^{3D} code.

Numerical Simulations

To illustrate various features of the SANICLAY model with destructuration in a boundary value problem, response of a saturated clay slope under dynamic excitation has been numerically simulated using this constitutive model integrated within the framework of FLAC^{3D}. Capabilities of the main features of the model in the constitutive level have been validated against a number of laboratory tests in our recent publications. For the current purpose, the model parameters used in the simulations are adopted from Dafalias et al. (2006), whereas the SANICLAY model with nonassociated flow rule had been calibrated for data of lower Cromer till (LCT) clay (Gens 1982). To also observe the effect of the destructuration mechanism in the present version of the model, it is assumed that $k_i = 0.6$ and $A = 0.5$. Details of the simulations and the results are presented and discussed in this section.

Physical Model Description

A 5H:1V slope of saturated clay is considered under self-weight, and simulation is conducted in FLAC^{3D} using the SANICLAY model described in previous sections. Fig. 2 shows the model dimensions and the mesh used in this study. The model is discretized using 1,700 brick zones in FLAC^{3D}. The zone length is smaller than 1/10 of the shortest wavelength (on the basis of elastic properties of the material and the input frequency) to provide accurate wave transmission. For simplicity, the grid points have been fixed in the y-direction and thus, the problem is reduced to only two dimensions (x-z). The analyses start with application of the initial stresses and hydrostatic pore pressures using a K_0 value of 0.6. On the basis of empirical charts by Brooker and Ireland (1965), this value of K_0 corresponds to the properties of LCT clay (effective angle of friction, $\phi' = 30°$; plasticity index, $I_p = 13\%$) with an assumed lightly overconsolidated state of overconsolidation ratio (OCR) $\approx$2. Starting from this stress state, the gravity is switched on and the models are brought to equilibrium. The slope remains stable under self-weight. The input excitation is then applied in the form of horizontal acceleration at the base of the model. The deformations that were created during the gravity application are reset to zero before the dynamic analysis. Fig. 3 shows the time history of the input acceleration with a frequency of 2 Hz and a maximum amplitude of 0.25 g.

The computational framework is based on the explicit finite-difference scheme to solve the full equations of motion, using lumped grid-point masses derived from the density of surrounding

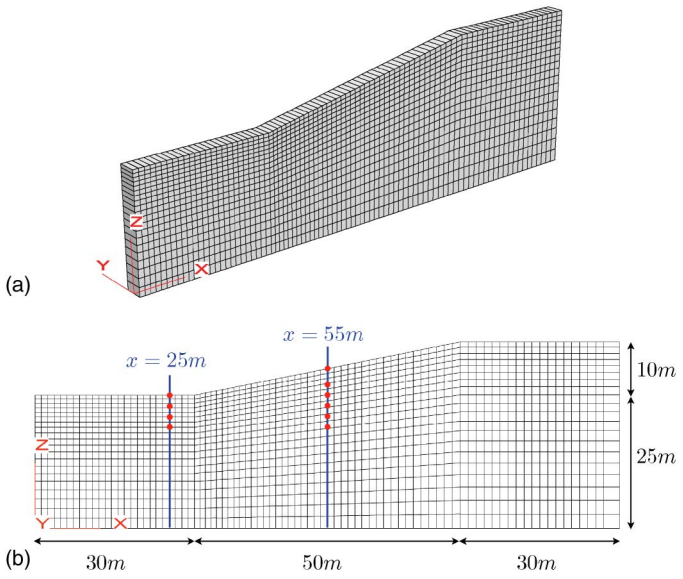

Fig. 2. Model geometry, the finite difference mesh, and the positions of the monitoring points

zones (rather than fictitious masses used for static solution). The dynamic feature is coupled to the groundwater flow model. The problem of interest in the current study, i.e., seismic response of saturated clayey slopes, is essentially an undrained problem, and this allows for the switching off of water flow in the analysis. A proper constitutive model and built-in equations for modeling of solid-fluid interaction allow the time-dependent pore-pressure changes in clayey ground. For the dynamic analyses, wave reflections at model boundaries are reduced by specifying the free-field boundary conditions of the sides. This approach enforces the free-field motion in such a way that boundaries retain their nonreflecting properties, i.e., outward waves are properly absorbed.

Results and Discussion

Three general sets of dynamic analyses have been conducted to study the response of the saturated slope under base acceleration. The model constants and the initial values of the model internal variables (at the beginning of the base excitation) used in these three analyses are presented in Tables 1 and 2 as Simulations I, II, and III. These simulations are outlined in the following sections.

Reducing SANICLAY to MCC

Simulation I uses the built-in MCC model (Roscoe and Burland 1968; Wood 1990) in FLAC^{3D}. The initial state of the only internal variable in the MCC model, p_0, is set to $p_0 = Rp_{0,n}$, with $p_{0,n}$ the corresponding value of p_0 for the normally consolidated state at the present stress state, i.e., having the stress point on the yield surface. A value of $R = 1.2$ has been used here for calculation of initial p_0 so that the material is slightly overconsolidated.

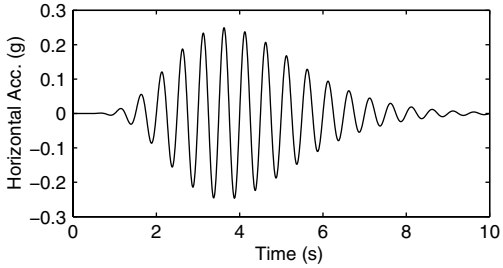

Fig. 3. Time history of input motion

Simulation II uses the newly implemented SANICLAY model but with proper parameters and internal variables such that the model's response is reduced back to the MCC model, i.e., with no Lode angle dependency ($m = 1$), no anisotropy ($\alpha = \mathbf{0}$, $C = 0$, $x = 1$), and no destructuration ($S_i = 1$ and/or $k_i = 0$). Detailed results of Simulations I and II are observed to be identical. As an example, time histories of shear stresses σ_{xz} and shear strains ϵ_{xz} for two locations in the model, namely ($x = 25$ m, $z = 23$ m) and ($x = 55$ m, $z = 27$ m), are presented in Fig. 4 and show the comparison between the results of Simulations I (solid lines) and II (circles). These two simulations illustrate the possibility of reducing the SANICLAY with destructuration to the well-known MCC simply by assigning proper values to model constants and internal variables. In addition, because the numerical implementation of the built-in MCC model in FLAC^{3D} has been already verified for different stress paths against the closed-form solutions (Itasca Consulting Group 2006), the observed identical results of MCC and the newly implemented SANICLAY could also be interpreted as another successful verification test for the numerical implementation of SANICLAY, in addition to the element test verifications presented in the previous section.

SANICLAY with Destructuration

Simulation III uses the complete set of model parameters and internal variables for the SANICLAY model with destructuration. The initial deviatoric stress state is used to estimate the initial value of the internal tensor variable α as $\mathbf{s}/x$. The initial size of yield surface is again set to $p_0 = Rp_{0,n}$ with $R = 1.2$; therefore, a small value of overconsolidation has been introduced for the material state at the beginning of the shaking phase. A number of representative results of Simulation III are presented in Figs. 5–9 and explained in the following paragraphs.

Referring to Fig. 2 for the coordinate definition, Figs. 5(a), 5(c), and 5(e) present the variations of shear stresses σ_{xz} and shear strains ϵ_{xz} at depths of 2 m ($z = 23$ m) and 6 m ($z = 19$ m) from the ground surface at the toe of slope ($x = 25$ m). Similarly,

Table 1. Model Constants Used in Simulations I, II, and III

Model constant		Simulation I (MCC)	Simulation II (SANICLAY)	Simulation III (SANICLAY)
Elasticity	κ	0.009	0.009	0.009
	ν	0.2	0.2	0.2
Critical state	M_c	1.18	1.18	1.18
	m	N/A	1	0.73
	λ	0.063	0.063	0.063
Hardening	C	N/A	0	16
	x	N/A	1	1.56
Destructuration	k_i	N/A	0	0.6

Table 2. Initial Values of the Model Internal Variables Used in Simulations I, II, and III

Model internal variables		Simulation I (MCC)	Simulation II (SANICLAY)	Simulation III (SANICLAY)
Size of the YS	p_0	$1.2p_{0,n}$	$1.2p_{0,n}$	$1.2p_{0,n}$
Orientation of the YS	α	N/A	0	$\mathbf{s}/x$
Structuration factor	S_i	N/A	1	3

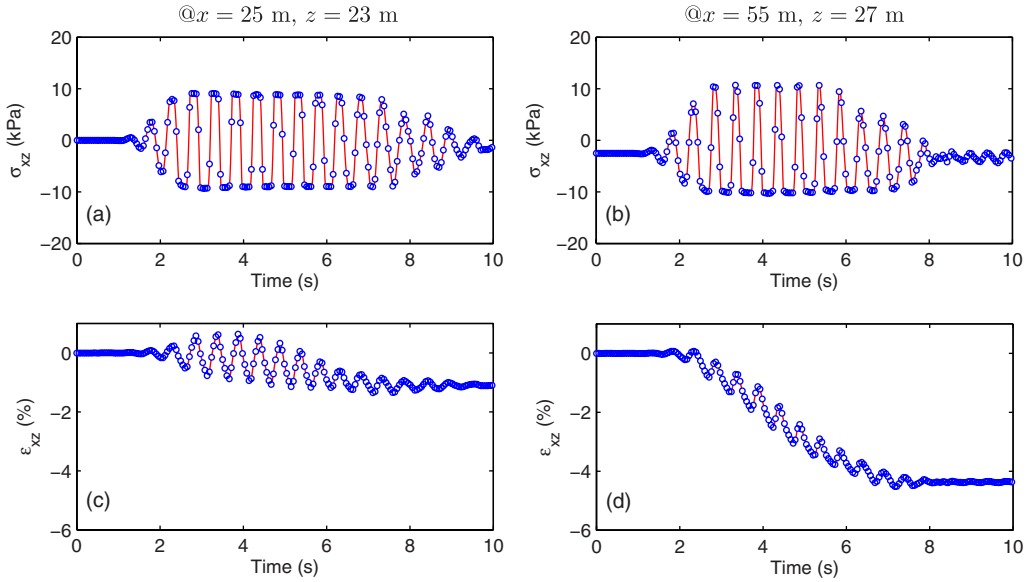

Fig. 4. Comparison of the time histories of shear stress σ_{xz} and shear strain ϵ_{xz} in Simulations I (solid lines) and II (circles) at two locations in the model

Figs. 5(b), 5(d), and 5(f) present these results at depths of 3 m ($z = 27$ m) and 7 m ($z = 23$ m) from the ground surface at the middle section of the slope ($x = 55$ m). The strain-softening regime of the response, particularly at shallower depths, is clear in these results. Plasticity, which leads to destructuration and softening of response, occurs in both directions of loading and reverse loading at $z = 25$ m (toe of the slope), whereas at $z = 55$ m (middle of the slope), it is primarily a one-sided cyclic plasticity. This is because of the larger value of the initial offset shear that exists in the sloping part of the model. The occurrence of plasticity can be detected by accumulation of the shear strains in Figs. 5(c)–5(f) as well as the (almost) flattening of the shear stresses in Figs. 5(a) and 5(b). Most of downslope accumulation of the plastic strains occurs in the sloping section. The magnitude of strain $|\epsilon_{xz}|$ reaches a value of 12% at $z = 27$ m in the middle of the slope ($x = 55$ m), whereas at the toe section ($x = 25$ m), it is on the order of 1–2%. To show the effect of the destructuration mechanism on shear stress/strain variations in the slope, similar plots to Figs. 5(e) and 5(f) are also presented in Fig. 6(a) and 6(b) for Simulations I or II. Comparison of these plots shows that the softening regime that is produced by the destructuration mechanism in Simulation III, and is missing in Simulations I and II, significantly affects the accumulation of shear strains.

Fig. 7 shows time histories of the shear strains ϵ_{xz}, horizontal displacements u_x, and structuration levels S_i at different depths in the middle of the slope ($x = 55$ m). In particular, the results close to the ground surface ($z = 30$ m) and at depths of 3 m ($z = 27$ m), 7 m ($z = 23$ m), 9 m ($z = 21$ m), and 13 m ($z = 17$ m) are presented in this figure. The residual value of the shear strain first increases by depth and then it diminishes again in the deeper parts of the section. Fig. 7(a) shows that $|\epsilon_{xz}|$ rises to about 13% at $z = 27$ m, whereas it does not exceed 9% and 5% close to the surface ($z = 30$ m) and at $z = 23$ m, respectively. This trend agrees well with the expected dynamic response observed in other numerical analyses. The pattern of variations of the structuration level S_i in Fig. 7(c) is similar to the patterns of variations of strains in Fig. 7(a) because the destructuration level is linked to the value of plastic strains, as presented in Eqs. (9) and (10). The values of horizontal displacements, however, continuously decrease with depth, as shown in Fig. 7(b). Displacements are a representation of the integration of strains in depth; hence, as long as strains accumulate in the downslope direction, regardless of their magnitude in each level, the resulting displacements increase by decreasing the depth. The maximum computed horizontal displacement in this section ($x = 55$ m) is at the surface and is about 1.25 m.

Contours of maximum shear strains and displacements throughout the model at 3, 5, 7, and 10 s are presented in Figs. 8 and 9. A map has been used at different times in each figure for easier comparison. The values have a consistent increasing pattern in time. The maximum shear strain reaches almost 12% at the end of shaking in a depth of about 3 m in the slope. This is large enough to bring the stress-strain response to the softening regime, owing to destructuration (e.g., see Fig. 5 for more details). There is also some strain concentration up to about 15% close to the toe of the slope. The displacement magnitude reaches a maximum value in the order of 1.3 m at the surface of the sloping part of the model.

As previously mentioned in all of the simulations presented in the "Numerical Implementation of the Model" section, an initial stress state corresponding to $K_0 = 0.6$ is assumed, and the focus is actually on the response in the dynamic excitation using different features of the model. Starting from the same initial stress state allows for the comparison of results; otherwise, the differences in response would be not only from the role of the constitutive model during the excitation phase, but also from what the constitutive model would dictate for the initial stress states under self-weight. However, one should not forget the strong capability of the SANICLAY model for realistic prediction of the K_0 value. Unlike the MCC model, which is known for overestimating the K_0 value, the SANICLAY can be calibrated through x to whatever is measured as the value of K_0.

Effects of Destructuration and Anisotropy

Two of the main interests in the current development are accounting for destructuration and anisotropy of clays in a numerical framework. There are two input factors that control the destructuration mechanism in the present model, the initial degree of structuration S_i and the rate of destructuration controlled by the constant k_i. The effects of these two factors on the computed maximum

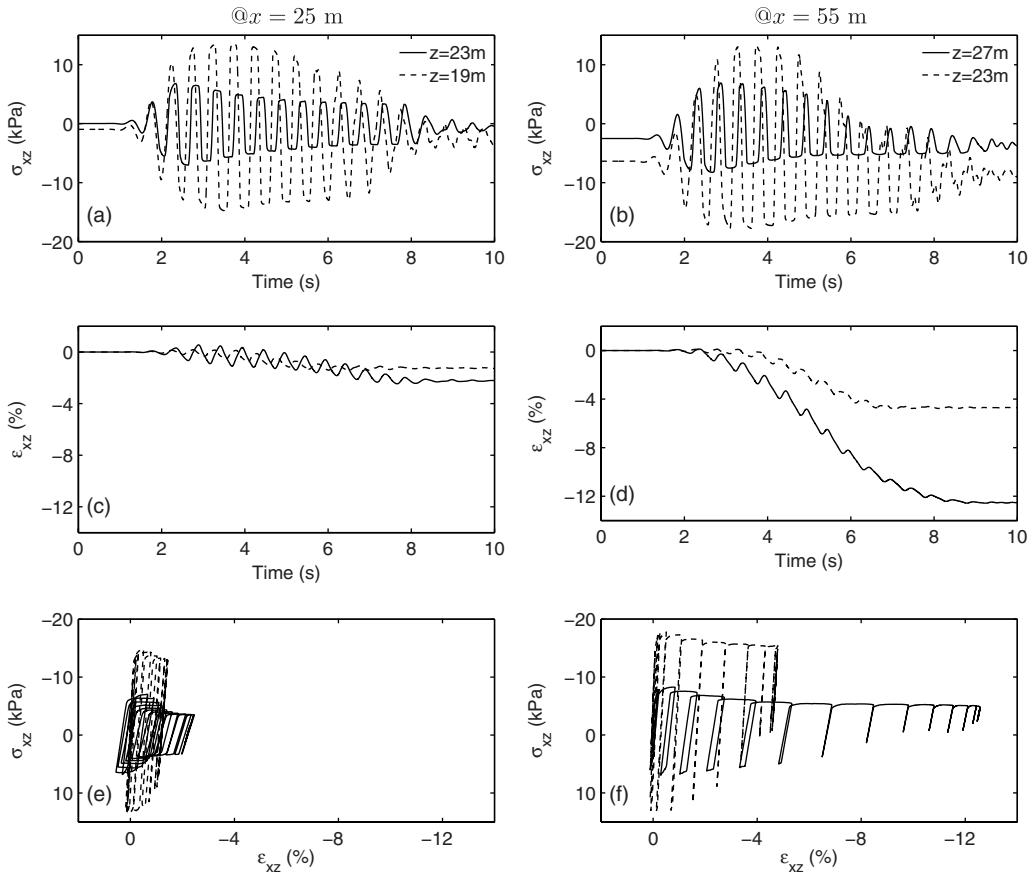

Fig. 5. Results of Simulation III for: (a), (b) shear stressσ_{xz} time histories; (c), (d) shear strain ϵ_{xz} time histories; and (e), (f) variations of σ_{xz} versus ϵ_{xz} at four different locations in the model

displacement is illustrated in Fig. 10. Ten different combinations of S_i and k_i are studied, and the resulting maximum displacements are shown in two different formats in Figs. 10(a) and 10(b). The analyses cover the cases with no initial structuration ($S_i = 1$) and with different initial structuration factors ($S_i = 1.5$, 2, and 3). Also, different rates of destructuration have been included in this study by assigning the values $k_i = 0.1$, 0.6, and 1.2. In the absence of structuration ($S_i = 1$) the maximum displacement is about 0.85 m. The presence of structuration ($S_i > 1$) increases this value, and for each initial value of S_i the rate of destructuration k_i plays a direct role on the permanent displacements. Depending on the level of initial structuration factor and the rate of destructuration, the resulting maximum displacement magnitude in this problem falls in the range of 0.85 to 1.4 m.

Figs. 11 and 12 show contours of maximum shear strain and displacement magnitude, respectively, at the end of shaking ($t = 10$ s) for simulations with different initial levels of structuration ($S_i = 1$, 1.5, and 3). For all of these simulations $k_i = 0.6$. In particular, Fig. 11(a) shows that in the absence of initial structuration, i.e., in simulation with the initial $S_i = 1.0$, the maximum shear strain at the end of shaking reaches about 8% in the slope. This value increases with the initial value of S_i, as is shown in Figs. 11(b) and 11(c), such that with initial values of $S_i = 1.5$ and 3.0 the maximum shear strain reaches approximately 10% and 15%, respectively. This is because larger values of initial structuration result in larger softening and reduction of strength, which in turn cause larger plastic shear strains in the slope. The same analogy applies to the displacements shown in Fig. 12. The magnitude of (downslope) displacement reaches about 0.85, 1.10, and 1.30 m for the initial values of $S_i = 1$ (no initial structuration), 1.5, and 3.0.

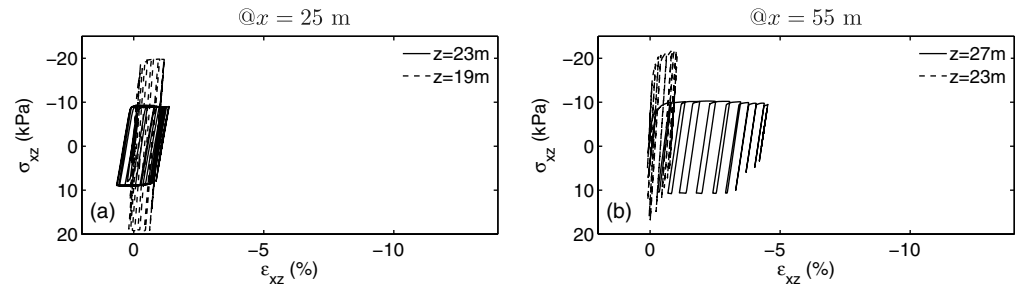

Fig. 6. Results of Simulation I or II (the same) for: (a), (b) shear stress variations of σ_{xz} versus ϵ_{xz} at four different locations in the model—to be compared with Fig. 5

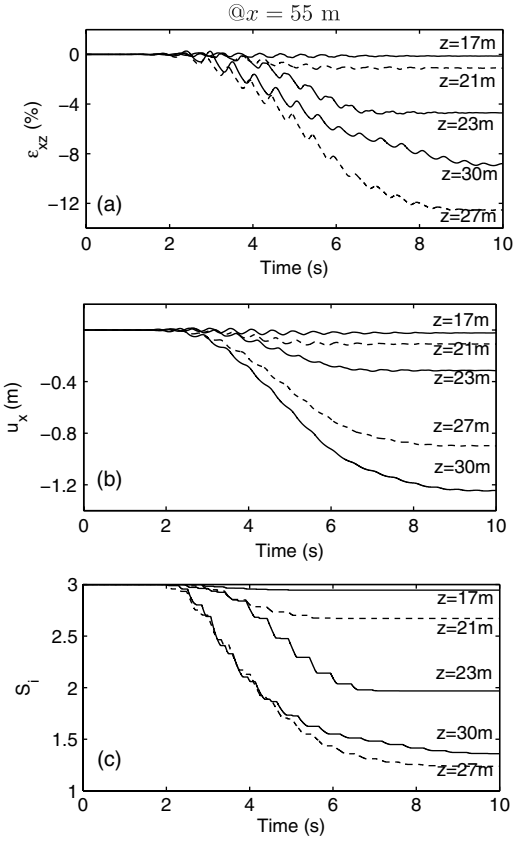

Fig. 7. Results of Simulation III for time histories: (a) shear strain ϵ_{xz}; (b) displacement u_x; and (c) S_i at five different depths in the middle section of the slope ($x = 55$ m)

Finally, time histories of the horizontal displacements at three different depths in the middle of slope ($x = 55$ m and $z = 30$, 27, and 25 m) are presented in Fig. 13. Different line styles in this figure are used to identify the initial levels of structuration S_i, and different symbols are used to identify the depths. This figure shows the accumulation of lateral displacements at these monitoring points during the 10 s of shaking. It can be observed that at each depth the displacements u_x increase with the initial level of structuration S_i. The amount of displacement is also a function of depth, as expected. In addition, the accumulation of horizontal displacements takes longer for larger initial values of S_i and also for shallower depths. The reason for longer lasting accumulation of displacements in shallower depths is probably because the shear waves reach the shallower depths later than the deeper ones. On the other hand, at the same depth, the reason for longer lasting displacement accumulations in the case of larger initial S_i values could originate from the more pronounced softening response, which results in reduction of strength (and may demand a kind of redistribution of stresses to bring the system to equilibrium). In the extreme case, if the strength after the softening regime falls considerably below the demanding stress for stability of the slope, the system might experience very large displacements and rotations that could be interpreted as failure of slope before it reaches a new redistribution of stresses (and geometry) in equilibrium. The issue of failure can happen in models with large S_i and can be absent in traditional models ($S_i = 1$). More accurate analysis of this kind of problem would require using the large strain mode of FLAC^{3D}, involving large displacements, displacement gradients, and rotations and would be a subject for further detailed studies.

For assessing the importance of the anisotropic (rotational) hardening in the model, one may compare results of simulation without anisotropic hardening ($C = 0$) with those of simulation II with anisotropic hardening ($C = 16$). The analyses show that the maximum value of displacement in the slope for the first case (without anisotropy, $C = 0$) is about 0.65 m, while in the second case (with anisotropy, $C = 16$) with a 30% increase it reaches as high as 0.85 m. Fig. 14 displays in more detail the effect of the rate of anisotropic hardening by variation of the parameter C in a range of 0 to 30 (typical range). The maximum values of displacements in the slope increase with the rate of evolution of anisotropy as illustrated in this figure. The effect of anisotropy may appear even more important in problems where two-sided cyclic plasticity is more pronounced.

Comparison with Engineering Techniques

In this section an attempt has been made to compare the results obtained from simulations in the previous section with those from engineering techniques. The method of dynamic slope stability analysis developed by Newmark (1965) and its variations and extensions are widely used in standard engineering practice and described by numerous writers (e.g., Seed 1979; Wilson and Keefer 1983; Finn et al. 1997; Rathje 1998; Kramer and Smith 1997; Kramer and Lindwall 2004; Pradel et al. 2005; Bray and Travasarou 2007). The Newmark analogy of a sliding block on a sloping plane combines two sets of data: (1) a critical acceleration, a_c, at which the slope would reach its ultimate strength and (2) an acceleration time history at the *site*. When the base

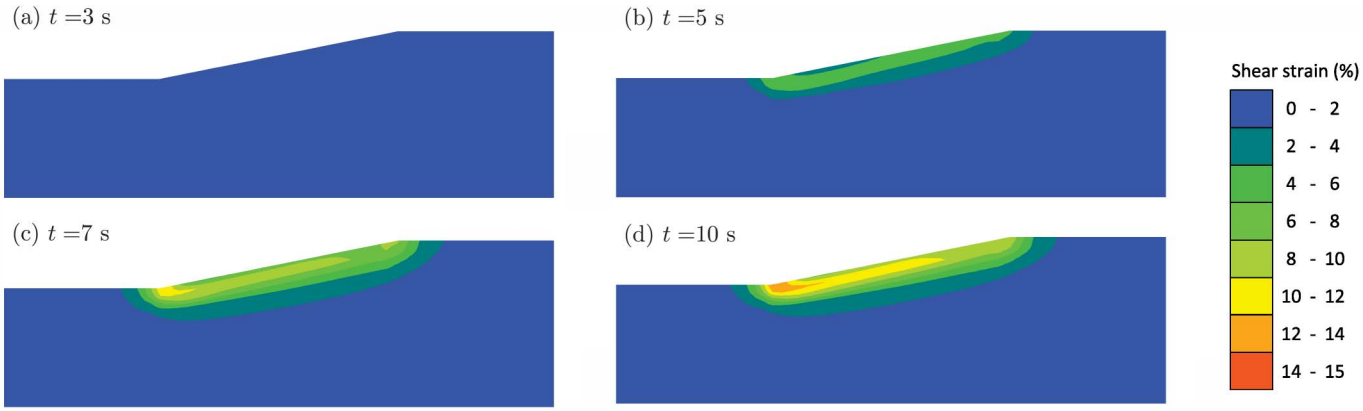

Fig. 8. Contours of maximum shear strain in Simulation III at four different times during the analysis

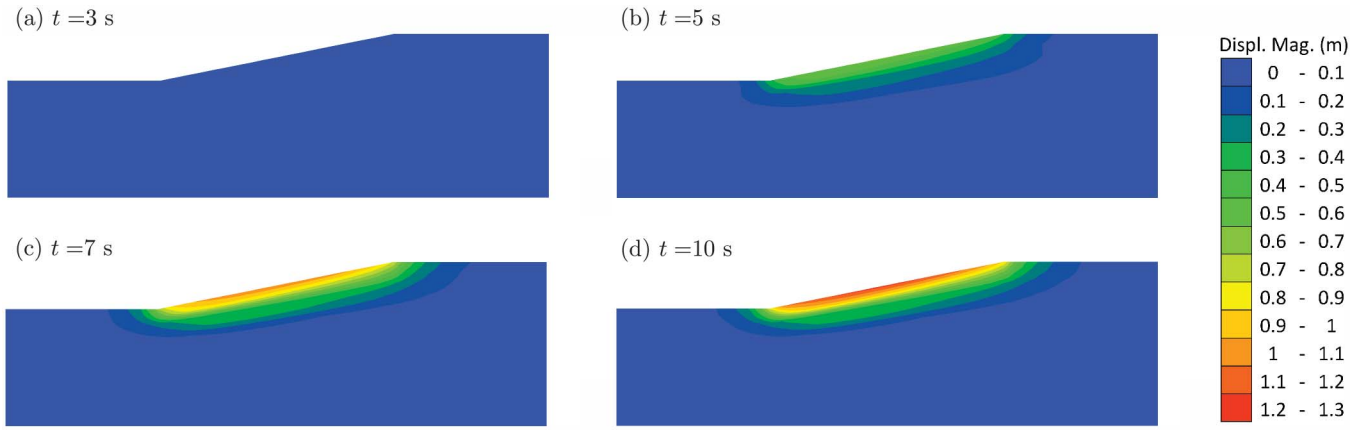

Fig. 9. Contours of displacement magnitudes in Simulation III at four different times during the analysis

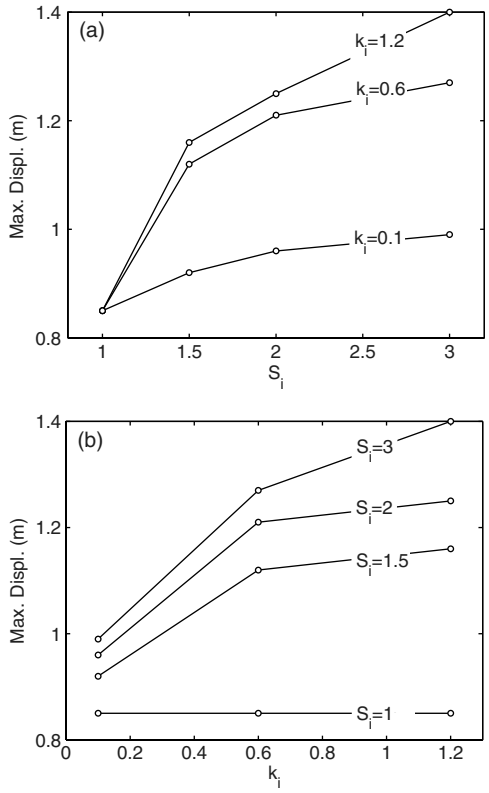

Fig. 10. Effect of destructuration on the maximum displacement magnitude in the model: (a) maximum displacement as function of structuration factor S_i; and (b) maximum displacement as function of the rate of destructuration k_i

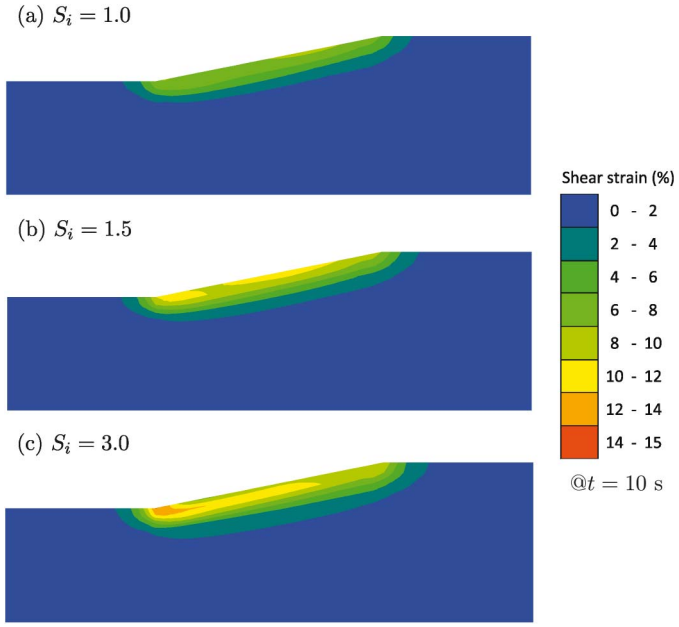

Fig. 11. Comparison of the contours of maximum shear strain for starting the analyses from: (a) $S_i = 1$ (no internal bonding); (b) $S_i = 1.5$; and (c) $S_i = 3$ (with $k_i = 0.6$)

acceleration time history exceeds the critical acceleration, the block slides. The total accumulated displacement is computed by double integration of the acceleration time history that exceeds the critical acceleration. Note that conventional Newmark-type analyses assume that the shear strength of a soil is unchanged during an earthquake. To account for strain softening of soil during shearing, Matasovic et al. (1997) have proposed an application of a degrading yield acceleration. To this end, when the downslope displacement increases from zero to δ_r, the yield acceleration can degrade linearly from a_{c1} to its residual value a_{c2} and then remain constant at this value.

To obtain the downslope displacement of the problem presented in the "Results and Discussion" section, some estimates of the engineering parameters of soil, namely, the elastic shear modulus G and undrained shear strength s_u, can be made as follows. The elastic shear modulus G (and the elastic bulk modulus K) can be extracted directly from Eq. (2) of the SANICLAY model. The equivalent undrained shear strength $s_u = Mp_{cs}/2$, where p_{cs} refers to the value of mean effective stress at the critical state, and M refers to the stress ratio at the critical state and depends on the Lode angle under which this undrained loading occurs. Assume that the initial state of soil in the SANICLAY model is characterized by p, p_0, and α. By making a reasonably good assumption that α does not change under undrained loading in compression, it can be shown that the equivalent undrained shear strength s_u is (Dafalias 1986; Wood 1990)

$$s_u = \frac{M}{2} p \left(\frac{p_0}{rp}\right)^{(\lambda-\kappa)/\lambda} \tag{17}$$

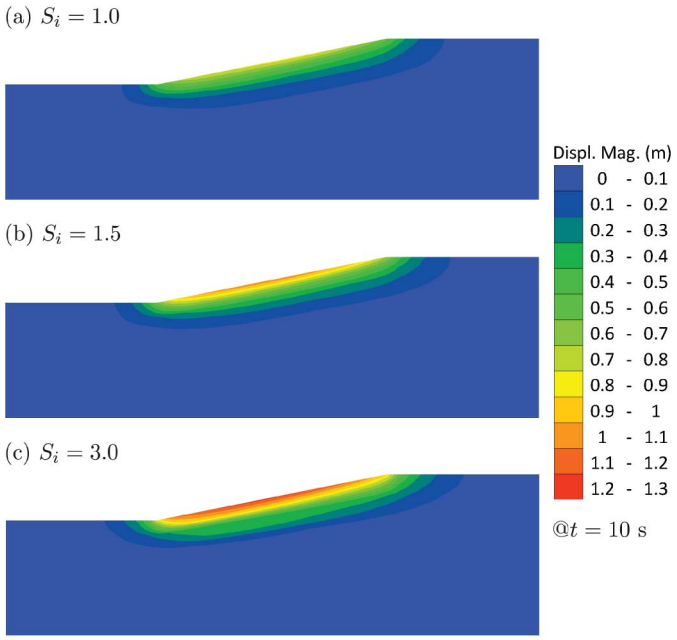

Fig. 12. Comparison of the contours of displacement magnitude for starting the analyses from: (a) $S_i = 1$ (no internal bonding); (b) $S_i = 1.5$; and (c) $S_i = 3$ (with $k_i = 0.6$)

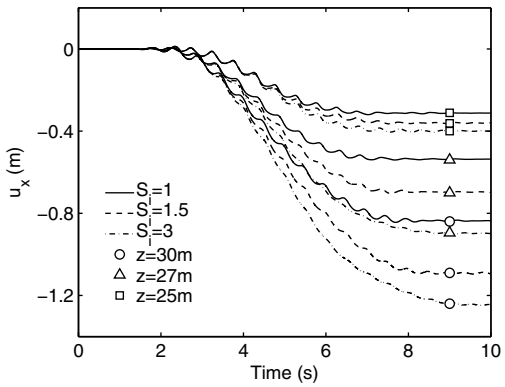

Fig. 13. Comparison of the time histories of horizontal displacement u_x at different locations in the middle part of the model ($x = 55$ m) for starting the analyses from different values of S_i

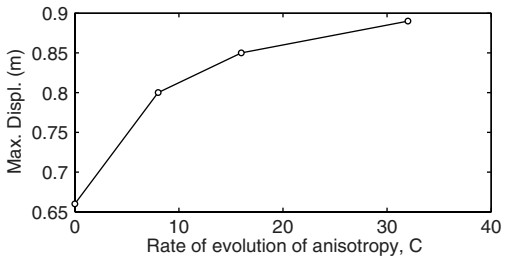

Fig. 14. Effect of the anisotropic hardening on the maximum displacement magnitude in the model

where the value of r for the SANICLAY model is $2M/(M + \sqrt{(3/2)\alpha : \alpha})$ and clearly depends on the current degree of anisotropy expressed through α, which was assumed to remain fixed. The value of r for the MCC model is 2.

With the equivalent values of elastic moduli and undrained shear strength at different depths of the model, it is possible to compute the factor of safety (FS) of the slope under self-weight by the conventional static slope stability methods. This has been done using the strength-reduction method (Dawson et al. 1999) that is implemented in FLAC^{3D}. It can be observed from the results presented in the "Results and Discussion" section that for the present mild slope, the failure mechanism under seismic loading may be approximated by a shallow translational regime. For a slope with angle θ, the critical acceleration a_c may be related to FS by (e.g., Wilson and Keefer 1983)

$$a_c = (\text{FS} - 1)g \sin\theta \tag{18}$$

where g = acceleration caused by gravity. In the present study, $\theta \simeq 11°$.

A key issue in this method is selection of the acceleration time history. To be consistent, one may rerun the slope model with the base acceleration using only the elastic parameters, as explained above. By putting one monitoring point on the flat surface downslope and one on the flat surface upslope, two acceleration time histories may be recorded. The reality is that the slope is subjected to something between these two. Alternatively, these two acceleration time histories may be calculated using only one-dimensional (1D) site response analyses on soil columns with the elastic shear modulus profile as obtained with the original model. The latter approach has been used here to produce the acceleration time histories $a_{x,u}$ and $a_{x,d}$ on the related upslope and downslope elevations, respectively; the results are shown in Fig. 15. It appears that the 25 m (downslope) and 35 m (upslope) of elastic soils amplify the peak acceleration from 0.25 g to 1.35 g and 1.0 g, respectively.

Table 3 summarizes the results of Newmark sliding-block analyses and those obtained from FLAC^{3D} with the SANICLAY model. The results of the investigation of five different cases are shown in this table.

In the first case, it is assumed that no degradation occurs in the strength of soil. The static factor of safety under self-weight is obtained as FS = 2.65. To this end, a Mohr-Coulomb (M-C) material model with variable undrained shear strength s_u at different depths is used [see Eq. (17)], and the value of FS is computed using the strength-reduction method. In this M-C model, it is assumed that friction angle and cohesion are $\phi = 0$ and $c = s_u$, respectively. The elastic bulk and shear moduli are extracted from the SANICLAY model. With the known FS = 2.65 the value of the critical acceleration can be computed from Eq. (18) as $a_c = 0.32$ g. Using the Newmark sliding-block method with this value of a_c and the measured acceleration time histories $a_{x,u}$ and $a_{x,d}$ (Fig. 15), the accumulated displacements are computed as 0.66 and 1.32 m, respectively. As in reality, the slope is subjected to something between these two values, the average of these two values, i.e., 0.99 m, is reported as the result of Newmark sliding-block analysis for this case. The corresponding maximum displacement from the

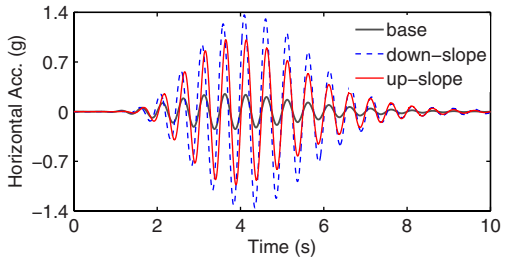

Fig. 15. Acceleration time histories at the base (same as Fig. 3), measured on the flat surface downslope ($a_{x,d}$), and on the flat surface upslope ($a_{x,u}$)

Table 3. Summary of Simulation Results from FLAC^{3D} and Newmark Sliding-Block Analyses

Description	FS	a_c	Max. displ. (m) Newmark (average)[a]	Max. displ. (m) FLAC^{3D}
No degradation of strength	2.65	0.32 g	0.99	0.85[b]
Fully degraded strength	1.87[c]	0.17 g	1.66	—
Destructuration	—	0.32 – 0.17 g	1.48 ($\delta_r = 0.2$ m) 1.36 ($\delta_r = 0.4$ m) 1.26 ($\delta_r = 0.6$ m)	1.12[d]
Fully degraded strength	1.46[e]	0.09 g	2.20	—
Destructuration	—	0.32 – 0.09 g	1.87 ($\delta_r = 0.2$ m) 1.66 ($\delta_r = 0.4$ m) 1.51 ($\delta_r = 0.6$ m)	1.22[f]

[a]The average of computed displacements using the acceleration time histories $a_{x,u}$ and $a_{x,d}$ (Fig. 15).
[b]SANICLAY with $S_i = 1$ or $k_i = 0$.
[c]In Eq. (17) p_{0d} is used instead of p_0, where $p_{0d} = p_0/S_i$ and $S_i = 1.5$.
[d]SANICLAY with $S_i = 1.5$ and $k_i = 0.6$.
[e]In Eq. (17), p_{0d} is used instead of p_0, where $p_{0d} = p_0/S_i$ and $S_i = 2.0$.
[f]SANICLAY with $S_i = 2.0$ and $k_i = 0.6$.

complete dynamic simulation in FLAC^{3D} using the SANICLAY model with $S_i = 1$ or $k_i = 0$ (for no strength degradation) is 0.85 m, as reported in the last column of the table for this case.

In the second case, the Newmark sliding-block analysis is repeated using a reduced $a_c = 0.17$ g. This value of a_c corresponds to a fully degraded soil strength when initially $S_i = 1.5$. To this end, the values of undrained shear strength in Eq. (17) are computed using $p_{0d} = p_0/S_i$ instead of p_0, resulting in a lower static FS and subsequently a lower a_c. The maximum displacement using the Newmark sliding-block analysis with this value of a_c is equal to 1.66 m, which is clearly larger than the 0.99 m in the first case.

In the third case, the Newmark sliding block is conducted using a variable critical acceleration from 0.32 g to 0.17 g. Depending on the rate of strength degradation (the relative displacement δ_r at which the critical acceleration drops to its residual value), different values of maximum displacement are obtained from the Newmark method. These values are to be compared with 1.12 m, which corresponds to the maximum displacement observed from complete dynamic simulation in FLAC^{3D} using the SANICLAY model with $S_i = 1.5$ and $k_i = 0.6$.

The fourth and fifth cases are similar to the second and third cases but with $S_i = 2.0$ instead of 1.5. No Newmark analysis corresponding to $S_i = 3.0$ is conducted here because the slope with fully degraded strength in this case is not stable under its self-weight.

Fig. 16 presents the time histories of horizontal displacement u_x obtained using Newmark sliding-block method (with the acceleration time histories $a_{x,d}$ and $a_{x,d}$, see Fig. 15) and SANICLAY model in FLAC^{3D}. In Fig. 16(a), a constant value of $a_c = 0.32$ g is used for the Newmark sliding-block calculations, and the resulting displacements can be compared with the horizontal displacements at the middle surface of the model analyzed in FLAC^{3D} using the SANICLAY model with $S_i = 1$ (no destructuration). In Fig. 16(b), however, the Newmark method uses a variable a_c that starts from 0.32 g and reduces linearly to 0.17 g when the displacement u_x increases from zero to δ_r. At larger displacements, the value of a_c remains constant at its residual level,

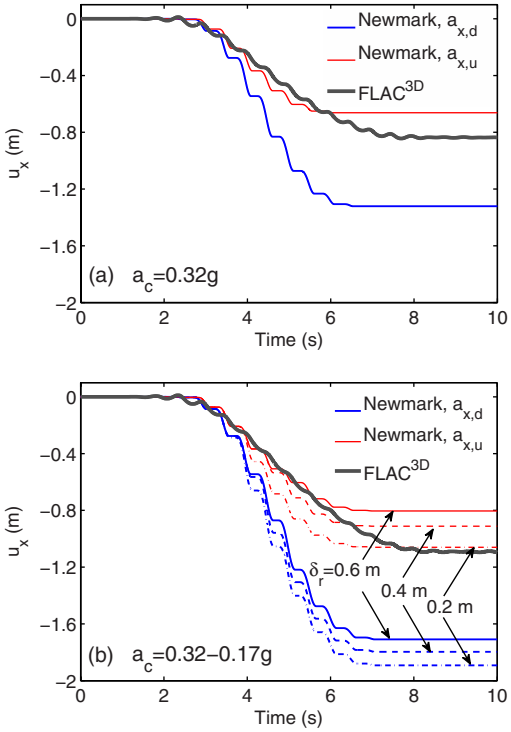

Fig. 16. Comparison of the time histories of horizontal displacement u_x using Newmark sliding-block method (with the acceleration time histories $a_{x,d}$ and $a_{x,u}$, see Fig. 15) and SANICLAY model in FLAC^{3D}: (a) constant a_c in Newmark method and no destructuration in SANICLAY model; (b) variable a_c in Newmark method and destructuration in SANICLAY model ($S_i = 1.5$)

i.e., 0.17 g. The results can be compared with those obtained from analysis of the slope in FLAC^{3D} using the SANICLAY model with destructuration ($S_i = 1.5$).

The overall comparison of the maximum displacements from the Newmark method and the complete analysis using the SANICLAY model shows that although the two analyses display the same trends, the modified Newmark sliding-block method provides conservative results compared with those obtained from the developed simulation model. Knowing that the equivalent natural frequency of 25–35 m of soil with the present properties is about 0.7 Hz, which is less than the frequency of the input motion, the observation of conservative results from the Newmark sliding-block method is consistent with the conclusion by Wartman et al. (2003). The presented results in Table 3 and Fig. 16 clearly emphasize the importance of inclusion of strain softening (destructuration) in the analyses. A similar trend was observed by Kaynia (2009) using a 1D model of seismic response of slopes with strain-softening behavior to highlight the significance of strain softening in performance-based design in geotechnical earthquake engineering.

Summary and Conclusions

This paper presents a comprehensive and yet simple version of the SANICLAY model built on the basis of its original more complete but also more complex formulation, which is described in Dafalias et al. (2006) and Taiebat et al. (2010). This model includes a number of key mechanisms that are essential in the prediction of response in clays, such as anisotropy and destructuration, in a simplified approach with the hope to make it attractive for real

applications. Capabilities of the main features of the model have been validated against a number of laboratory results in the writers' recent publications. The model without the destructuration features uses only two more parameters than the classical MCC model, and as a result it can capture the very important K_0 consolidation response, which the MCC is unable to provide, and the anisotropic effect induced by it. Destructuration can be accounted at the expense of two additional parameters, and this is very important for sensitive clays' response. The model has been efficiently integrated into the FLAC^{3D} program, which is known in both the research and practical communities of geotechnical engineering and especially in the field of geotechnical earthquake engineering. The implementation details have been extensively verified in the numerical framework. The general 3D implementation in this framework allows the developed framework to be used 3D fully coupled dynamic analysis of clay deposits and dynamic soil-structure interaction problems with arbitrary soil geometry and general 3D structures.

To demonstrate the importance of a number of key features of the model in simulation of boundary value problems, the resulting numerical framework has been used in modeling the seismic response in a slope problem. For simplicity of discussions, a 2D section of a slope created by 3D elements has been studied. The model acquires the reduced form of the classical MCC model by setting proper model constants. The influence of anisotropy and destructuration mechanisms in the simulation of the boundary-value problem has been demonstrated in this numerical study by repeating the analysis with these mechanisms activated and deactivated. When anisotropy and destructuaration are deactivated, in which case the model becomes the classical MCC model, the analysis may underpredict the rate of accumulation and the final level of plasticity that manifest in the developed permanent shear strains and the resulting deformations. This also includes the level of excess pore pressures developed owing to volumetric shear strains in the model and could be of interest in certain problems.

Comparison of the rigorous finite-difference results with a modified version of Newmark, in which the yield acceleration is gradually reduced as block sliding progresses during the earthquake, and the striking sensitivity of the results to this feature, emphasize the importance of inclusion of strain softening (destructuration) in the analyses. A similar trend was observed by Kaynia (2009) using a ID model of seismic response of slopes with strain-softening behavior to highlight the significance of strain softening in performance-based design in geotechnical earthquake engineering

Additional refinements of the model to more efficiently account for cyclic loading applicable to seismic problems and maintaining its simplicity are under way. However, the present framework meets a good portion of the practical needs, particularly in the offshore designs.

References

Andersen, K. H. (2009). "Bearing capacity under cyclic loading—Offshore, along the coast and on land." *Can. Geotech. J.*, 46(5), 513–535.

Argyris, J. H., Faust, G., Szimmat, J., Warnke, E. P., and Willam, K. J. (1974). "Recent developments in the finite element analysis of prestressed concrete reactor vessels." *Nucl. Eng. Des.*, 28(1), 42–75.

Bardet, J. P., and Choucair, W. (1991). "A linearized integration technique for incremental constitutive equations." *Int. J. Numer. Anal. Meth. Geomech.*, 15(1), 1–19.

Borja, R. I. (1991). "Cam—Clay plasticity, Part II: Implicit integration of constitutive equation based a nonlinear elastic stress predictor." *Comput. Methods Appl. Mech. Eng.*, 88(2), 225–240.

Borja, R. I., and Lee, S. R. (1990). "Cam—Clay plasticity, Part I: Implicit integration of elastoplastic constitutive relations." *Comput. Methods Appl. Mech. Eng.*, 78(1), 49–72.

Bray, J. D., and Rathje, E. M. (1998). "Earthquake-induced displacements of solid-waste landfills." *J. Geotech. Geoenviron. Eng.*, 124(3), 242–253.

Bray, J. D., and Travasarou, T. (2007). "Simplified procedure for estimating earthquake-induced deviatoric slope displacements." *J. Geotech. Geoenviron. Eng.*, 133(4), 381.

Brooker, E., and Ireland, H. (1965). "Earth pressures at rest related to stress history." *Can. Geotech. J.*, 2(1), 1–15.

Crisfield, M. A. (1991). *Non-linear finite element analysis of solids and structures. Vol. 1: Essentials*, Wiley, New York.

Dafalias, Y. F. (1986). "An anisotropic critical state soil plasticity model." *Mech. Res. Commun.*, 13(6), 341–347.

Dafalias, Y. F., Manzari, M. T., and Papadimitriou, A. G. (2006). "SANICLAY: simple anisotropic clay plasticity model." *Int. J. Numer. Anal. Meth. Geomech.*, 30(12), 1231–1257.

Dawson, E., Roth, W., and Drescher, A. (1999). "Slope stability analysis by strength reduction." *Géotechnique*, 49(6), 835–840.

Finn, W., Ledbetter, R., and Marcuson, W. III. (1997). "North American practice for evaluating the seismic safety of embankment dams." *Proc., 1st Int. Conf. on Earthquake. Geotechnical Engineering*, Balkema, Rotterdam, Netherlands, 1227–1251.

Finn, W. D. L., Martin, G. R., and Lee, K. W. (1977). "An effective stress model for liquefaction." *J. Geotech. Engrg. Div.*, 103(6), 517–533.

Gens, A. (1982). "Stress—strain and strength of a low plasticity clay." Ph.D. thesis, Imperial College, London University, 856.

Gens, A., and Nova, R. (1993). "Conceptual bases for a constitutive model for bounded soils and weak rocks." *Geomechanical engineering of hard soils and soft rocks*, A. Anagnostopoulos, F. Schlosser, N. Kaltesiotis, and R. Frank, eds., Balkema, Rotterdam, Netherlands, Vol. 1, 485–494.

Itasca Consulting Group, Inc. (2006). *FLAC3D—Fast Lagrangian analysis of continua in three dimensions, Ver. 3.1, User's manual*, Minneapolis.

Iwan, W. D. (1967). "On a class of models for the yielding behavior of continuous and composite systems." *J. Appl. Mech.*, 34(2), 612–617.

Jeremić, B., and Sture, S. (1997). "Implicit integrations in elasto-plastic geotechnics." *Mech. Cohes.-Frict. Mater*, 2, 165–183.

Kaynia, A. M. (2009). "Role of soil investigation in performance based design." *Performance-based design in earthquake geotechnical engineering: From case history to practice*, T. Kokusho, Y. Tsukamoto, and M. Yoshimine, eds., Taylor and Francis, London, 249–251.

Kramer, S., and Lindwall, N. (2004). "Dimensionality and directionality effects in Newmark sliding block analyses." *J. Geotech. Geoenviron. Eng.*, 130(3), 303.

Kramer, S., and Smith, M. (1997). "Modified Newmark model for seismic displacements of compliant slopes." *J. Geotech. Geoenviron. Eng.*, 123(7), 635.

Masing, G. (1926). "Eiganspannungen und verfestigung beim messing." *Proc., 2nd Int. Congress of Applied Mechanics*, Zürich, Switzerland, 332–335.

Matasovic, N., Kavazanjian, E., and Yan, L. (1997). "Newmark deformation analysis with degrading yield acceleration." *Proc., Geosynthetics*, Long Beach, CA, 989–1000.

Mroz, Z. (1967). "On the description of anisotropic workhardening." *J. Mech. Phys. Solids*, 15(3), 163–175.

Newmark, N. (1965). "Effects of earthquakes on embankments and dams." *Géotechnique*, 15(2), 139–160.

Nova, R. (1992). "Mathematical modelling of natural and engineered geomaterials." *Eur. J. Mech. A. Solids*, 11, 135–154.

Potts, D. M., and Gens, A. (1985). "A critical assessment of methods of correcting for drift from the yield surface in elastoplastic finite element analysis." *Int. J. Numer. Anal. Meth. Geomech.*, 9(2), 149–159.

Pradel, D., Smith, P., Stewart, J., and Raad, G. (2005). "Case history of landslide movement during the Northridge earthquake." *J. Geotech. Geoenviron. Eng.*, 131(11), 1360–1369.

Puzrin, A., Frydman, S., and Talesnick, M. (1995). "Normalized nondegrading behavior of soft clay under cyclic simple shear loading." *J. Geotech. Eng.*, 121(12), 836–843.

Ramberg, W., and Osgood, W. R. (1943). "Description of stress-strain curves by three parameters." *The Earth Technology Corporation. Technical Note No. 902*, National Advisory Committee For Aeronautics, Washington, DC.

Roscoe, K. H., and Burland, J. B. (1968). "On the generalized stress-strain behaviour of wet clay." *Engineering plasticity*, Cambridge University Press, Cambridge, UK, 553–609.

Seed, H. B. (1979). "19th Rankine lecture—Considerations in the earthquake resistant design of earth and rockfill dams." *Géotechnique*, 29(3), 215–263.

Sloan, S. W. (1987). "Substepping schemes for the numerical integration of elastoplastic stress-strain relations." *Int. J. Numer. Methods Eng.*, 24(5), 893–911.

Sloan, S. W., Abbo, A. J., and Sheng, D. (2001). "Refined explicit integration of elastoplastic models with automatic error control." *Eng. Comput.*, 18(1–2), 121–154.

Taiebat, M., Dafalias, Y. F., and Peek, R. (2010). "A destructuration theory and its application to SANICLAY model." *Int. J. Numer. Anal. Meth. Geomech.*, 34(10), 1009–1040.

Wartman, J., Bray, J., and Seed, R. (2003). "Inclined plane studies of the Newmark sliding block procedure." *J. Geotech. Geoenviron. Eng.*, 129(8), 673–684.

Wilson, R., and Keefer, D. (1983). "Dynamic analysis of a slope failure from the 6 August 1979 Coyote Lake, California, earthquake." *Bull. Seismol. Soc. Am.*, 73(3), 863–877.

Wood, D. M. (1990). *Soil behaviour and critical state soil mechanics*, Cambridge University Press, Cambridge, UK.